SUPPORTING INFORMATION

SI MATERIALS AND METHODS

Biological material and sequencing libraries. Buffy coats from healthy donors were purchased from Indiana Blood Center and all participants signed a written consent. The ethics committee at the CHU Sainte-Justine approved the project (protocol #4023). Peripheral blood mononuclear cells (PBMCs) were obtained by centrifugation on Ficoll-Paque, and monocytes were isolated by positive selection with CD14 magnetic beads (Miltenyi Biotec). Monocytes were differentiated into either DCs by adding rhIL-4 (20 ng/mL; Shenandoah Biotechnology,Inc) and rhGM-CSF (20 ng/mL; R&D Systems Inc.) or macrophages by adding rhM-CSF (20ng/mL; R&D Systems Inc.) in the cell culture medium.

DCs were infected with MTB for 2, 4, 5, 6, 18, 24, 48, and 72 h at a multiplicity of infection (MOI) of 1:1 or with heat-killed MTB at MOI of 5:1, as this MOI induces virtually the same transcriptional response at all four time points compared to that observed with live MTB (***SI Appendix,* Fig. S2**). Macrophages were infected with MTB in the same fashion as DCs or with *Salmonella typhimurium* as previously described (1). Briefly, macrophages were infected at MOI of 10:1 for 2 hours, washed, and cultured for 1 hour with 50μg/ml gentamycin, then washed again and cultured in complete medium with 3μg/ml gentamycin for an additional 2, 4, 8, 12, 24 or 48 h, the time points we refer to in the main text.

DNA from DCs was extracted using the PureGene DNA extraction kit (Gentra Systems). DNA from macrophages was extracted using the DNeasy Blood and Tissue Kit (Qiagen). RNA was extracted using the miRNeasy mini kit (Qiagen). RNA quality was evaluated with the 2100 Bioanalyzer (Agilent Technologies) and only samples with no evidence of RNA degradation (RNA integrity number > 8) were kept for further experiments.

ATAC-seq libraries were generated from 50,000 cells, as previously described (2). We collected ChIP-seq data for the H3K27ac histone mark in non-infected and *Salmonella*-infected macrophages as previously described (3). Sequencing was performed using the Illumina HiSeq 2500, as per the manufacturer's instructions.

TLR and Dectin-1 stimulations were performed on DCs with LPS (100 and 500 ng/mL, InvivoGen), gardiquimod (0.5, 1 and 2 ug/mL, InvivoGen), poly I:C (10, 20 and 30 ug/mL, InvivoGen) and beta-glucan (kindly provided by Dr. David Williams, University of Tennessee).

SeqCap Epi library preparation and sequencing. Libraries were generated as for the whole-genome sequencing with KAPA Library Preparation Kit for Illumina Platforms (KAPA Biosystems), as per the manufacturer's instructions. Library quality was assessed by 2100 Bioanalyzer (Agilent Technologies). Samples showing the desired profile were pooled together in equal mass according to Qubit quantification. We then performed a hybridization using the SeqCap Epi kit (Roche NimbleGen). The sample pool, indexes corresponding to the sequences of the adapters used for library preparation, and repetitive DNA (C_0t) were desiccated and then incubated in hybridization buffer with a set of customized probes for 72 hours to select and sequence target regions only. Specifically, DNA methylation data was collected for 33,059 target regions spanning >130,000 CpG sites (mean length = 300 bp; mean number of CpG sites = 5), which is less than 1% of the ~28 million CpGs contained in the human genome. These regions were primarily comprised of MTB-induced differentially methylated regions identified at 18 hours post-infection using whole-genome bisulfite sequencing, as well as other distal regulatory elements in DCs where changes in DNA methylation have been shown to be most likely to occur (***SI Appendix,* Fig. S1*A***) (3). Moreover, these candidate regions were nearby differentially expressed genes in response to MTB at 18 hours. Probes targeting a two kilobase region between coordinates 4500 and 6500 bp of the lambda genome (NC_001416.1) were also included in the SeqCap Epi design, as a control for bisulfite

conversion efficiency. Sequencing was performed using the Illumina HiSeq 2500, as per the manufacturer's instructions.

Whole-genome library preparation, sequencing and analysis. Libraries were generated with KAPA Library Preparation Kit for Illumina Platforms (KAPA Biosystems), as per the manufacturer's instructions. Briefly, genomic DNA was fragmented to 100-300 bp with an S2 sonicator (Covaris). Fragments were then end-repaired, A-tailed, and ligated with methylated sequencing adapters. Between every enzymatic step, libraries were purified using AMPure beads (Agencourt). After ligation, in addition to the AMPure bead purification, a DUAL-SPRI size selection was performed to further select for fragments with adapters in the window of 200-400 bp. Sodium bisulfite conversion was performed with EZ DNA Methylation Lightning Kit (Zymo Research), and libraries were amplified using KAPA Hifi HotStart Uracil Tolerant Enzyme (KAPA Biosystems). Library quality was assessed by 2100 Bioanalyzer (Agilent Technologies). Sequencing was performed on an S2 flowcell on an NovaSeq (Illumina), as per the manufacturer's instructions.

SeqCap Epi data processing and differential methylation analysis. Adaptor sequences and low-quality score bases (Phred score < 20) were first trimmed using Trim Galore (http://www.bioinformatics.babraham.ac.uk/projects/trim_galore/). The resulting reads were mapped to the human reference genome (GRCh37/hg19) and lambda phage genome using Bismark (4), which uses Bowtie 2 (5) and a bisulfite converted reference genome for read mapping. Only reads that had a unique alignment were retained. Methylation levels for each CpG site were estimated by counting the number of sequenced C ('methylated' reads) divided by the total number of reported C and T ('unmethylated' reads) at the same position of the reference genome using Bismark's methylation extractor tool. We performed a strand-independent analysis of CpG methylation where counts from the two Cs in a CpG and its reverse complement (position i on the plus strand and position i+1 on the minus strand) were combined and assigned to the position of the C in the plus strand. To assess MethylC-seq bisulfite conversion rate, the

frequency of unconverted cytosines (C basecalls) at lambda phage CpG reference positions was calculated from reads uniquely mapped to the lambda phage reference genome. Overall, bisulfite conversion rate was >99% in all of the samples (***SI Appendix,* Table S1**).

In DCs, differentially methylated (DM) CpG sites at each time point following MTB infection were identified using the R package DSS (6). We used a linear model with the following design: *DNA methylation ~ Donor + Infection*, which allowed us to consider the paired nature of the experiment and capture the effects of infection on DNA methylation observed within donors. We considered a CpG site as differentially methylated if statistically supported at a False Discovery Rate (FDR) < 0.01 and an absolute mean methylation difference above 10%. Only CpG sites that had a coverage of at least 5X in each of the samples were included in the analysis (103,649 in total).

To identify DM sites that show a stable loss of methylation (as Cluster 3 DM sites in DCs) in *Salmonella*-infected macrophages using one individual, we performed a hierarchical clustering analysis on sites that specifically: (*i*) do not change methylation at 2 hours (|methylation difference| < 10%), and (*ii*) lose methylation at 48 hours (methylation difference < -40%).

BS-seq data processing and promoter analysis

We used Trim Galore (http://www.bioinformatics.babraham.ac.uk/projects/trim_galore/) to trim off adapter sequences incorporated in the read and remove bases with a Phred base quality score below 20. The resulting reads were mapped to the human reference genome (GRCh37/hg19) and lambda phage genome using Bismark (4), which uses Bowtie 2 (5) and a bisulfite converted reference genome (C-to-T and a G-to-A) for read mapping. Only reads that had a unique alignment and a maximum of one mismatch were retained. PCR duplicates were removed using a Perl script that is part of the Bismark package (deduplicate_bismark_alignment_output.pl). The context of each C was determined, which allowed us to classify each C of the genome as CpG, CHH, or CHG, where H is either an A, T, or C

nucleotide. Methylation levels for each CpG site were estimated by counting the number of reported C ('methylated' reads) divided by the total number of reported C and T ('methylated' plus 'unmethylated' reads) at the same position of the reference genome using Bismark's methylation extractor tool. The same strategy was also applied for non-CpG methylation (CHG context, where H is either an A, T, or C nucleotide). We performed a strand-independent analysis of CpG methylation where counts from the two Cs in a CpG and its reverse complement (position *i* on the plus strand and position *i*+1 on the minus strand) were combined and assigned to the position of the C in the plus strand.

The summarized methylation estimates of strand-merged CpG sites from the 3 infected and 3 non-infected samples were used to identify MTB-induced differences in methylation at promoters, using the R package DSS (6), which implements the Bsmooth smoothing method (7). To minimize noise in methylation estimates due to low-coverage data, we restricted the differential methylation analysis to CpG sites with an average coverage of ≥4 sequence reads across all DC samples.

5hmC enrichment at DM sites. To calculate the enrichment of 5-hydroxymethylcytosine (5hmC) at DM CpG sites (Clusters 1, 2 and 3), we compared the distribution of 5hmC levels in non-infected DCs between DM and non-DM sites. Since non-DM sites have lower overall levels of baseline methylation than DM sites **(*SI Appendix,* Fig. S16A)**, we performed similar enrichment analysis by using a random set of non-DM sites that matches the distribution of methylation found in non-infected samples within each set of DM sites **(*SI Appendix,* Fig. S16B)**. Each random set contains the same number of CpG sites as those identified within each DM cluster.

RNA-seq data processing and identification of differentially expressed genes. Read count estimates per gene were obtained using the alignment-free method Kallisto (8). For all downstream analyses, we excluded non-coding and lowly-expressed genes with an average read count lower than 10 in all of the samples, resulting in 13,955 genes in total. The R package DESeq2 (9) was used to identify differences in

expression levels between non-infected and infected samples at each time point. Nominal p-values were corrected for multiple testing using the Benjamini-Hochberg method (10). The complete list of differentially expressed genes can be found in ***SI Appendix,* Dataset S3**. Differentially expressed genes in response to MTB were classified into 6 distinct temporal expression clusters: (i) **Early induced** genes, which show the highest level of expression at 2 hours post-infection and return back to basal levels; (ii) **Intermediate induced** genes, which show the highest level of expression at 18 hours post-infection and return back to basal levels; and (iii) **Persistent induced** genes, which become increasingly up-regulated over the course of infection. The same definition criteria was used for down-regulated genes.

Gene set enrichment analysis. We used ClueGO (11) at default parameters to test for enrichment of functionally annotated gene sets among differentially expressed genes. The results for these enrichment analyses are reported in ***SI Appendix,* Dataset S4**. Enrichment p-values were based on a hypergeometric test using the set of 13,955 genes as background. Benjamini-Hochberg method was applied for multiple testing correction.

ChIP-seq data processing and tag density profiles. ChIP-seq reads were trimmed for adapter sequences and low-quality score bases using Trim Galore. The resulting reads were mapped to the human reference genome using Bowtie 2 with the following option: -N 1. Only reads that had a unique alignment were retained, and PCR duplicates were further removed using Picard tools (http://broadinstitute.github.io/picard/). Tag density profiles for chromatin modifications and genome accessibility patterns around regions of interest were accomplished with ngs.plot package (12) using default parameters.

ATAC-seq data processing and TF footprinting analysis. ATAC-seq reads were trimmed for adapter sequences and low-quality score bases and were mapped to the human reference genome. Mapping was performed using BWA-MEM (13) in paired-end mode at default parameters. Only reads that had a unique

alignment (mapping quality > 10) were retained. TF footprinting analyses were performed as previously described, using the Centidual algorithm (3) and JASPAR annotated human TF binding motifs (2018 release) (14). For each of the actively bound TFs in DCs (241 in total; FDR < 0.05 at 18 hours post-infection; ***SI Appendix,* Dataset S5**)), we first trained Centidual assuming that the footprint was bound in the two conditions. Then, we fixed the model parameters and generated a likelihood ratio and posterior probability π_{lt} for each condition t separately and for each site l. To detect if the footprint was more active in one of the two conditions, we fit a logistic model that included an intercept for each condition (α and δ), the PWM effect β, and PWM times the treatment effect γ :

$$\log\left(\frac{\pi_{lt}}{1-\pi_{lt}}\right) = \alpha \times (1 - I_t) + \beta \times \text{PWMscore}_l + \delta \times I_t + \gamma \times (I_t \times \text{PWMscore}_l)$$

where I_t is an indicator variable that takes the value 1 if t = "treatment" and 0 if t = "control". We then calculated a Z-score for the interaction effect γ, corresponding to the evidence for condition-specific binding. ATAC-seq samples were down-sampled to obtain similar number of reads between NI and HI samples at each time-point. We used a window size of 300 bp on either side of the motif match, and reads with fragment lengths [40, 140] and [141, 600] bp for footprinting analyses.

To test for differential binding of immune-related TFs (NF-κB/Rel, AP-1, STATs, and IRFs) between non-infected and infected samples, we compared the intensity of the Tn5 sensitivity-based footprint across all matches to motifs of TFs that belong to each family in the hypomethylated regions. Motif IDs (and corresponding names) were aggregated to their respective TF family as follows:

NF-κB/Rel	
MA0105.3	NFKB1
MA0105.2	NFKB1
MA0105.1	NFKB1
MA0105.4	NFKB1
MA0778.1	NFKB2
MA0101.1	REL
MA0107.1	RELA
MA1117.1	RELB

AP-1	
MA0833.1	ATF4
MA0834.1	ATF7
MA0462.1	BATF::JUN
MA0835.1	BATF3
MA0476.1	FOS
MA0099.3	FOS::JUN
MA1126.1	FOS::JUN(var.2)
MA1134.1	FOS::JUNB
MA1141.1	FOS::JUND
MA1127.1	FOSB::JUN
MA1135.1	FOSB::JUNB
MA1136.1	FOSB::JUNB(var.2)
MA0477.1	FOSL1
MA1128.1	FOSL1::JUN
MA1129.1	FOSL1::JUN(var.2)
MA1137.1	FOSL1::JUNB
MA1142.1	FOSL1::JUND
MA1143.1	FOSL1::JUND(var.2)
MA0478.1	FOSL2
MA1130.1	FOSL2::JUN
MA1131.1	FOSL2::JUN(var.2)
MA1138.1	FOSL2::JUNB
MA1139.1	FOSL2::JUNB(var.2)
MA1144.1	FOSL2::JUND
MA1145.1	FOSL2::JUND(var.2)
MA0655.1	JDP2
MA0656.1	JDP2(var.2)
MA0488.1	JUN
MA0489.1	JUN(var.2)
MA1132.1	JUN::JUNB
MA1133.1	JUN::JUNB(var.2)
MA0490.1	JUNB
MA1140.1	JUNB(var.2)
MA0491.1	JUND

STATs	
MA0137.1	STAT1
MA0137.2	STAT1
MA0137.3	STAT1
MA0517.1	STAT1::STAT2
MA0144.2	STAT3

IRFs	
MA0050.2	IRF1
MA0050.1	IRF1
MA0051.1	IRF2
MA1418.1	IRF3
MA1419.1	IRF4
MA1420.1	IRF5
MA0772.1	IRF7
MA0652.1	IRF8
MA0653.1	IRF9

To test for enrichment of binding of methylation-sensitive ("methyl-minus") TFs in hypomethylated regions, we compared the proportion of regions that overlap well-supported footprints (posterior probability > 0.99) of "methyl-minus" TFs reported in Yin *et al.* (15)) among non-DMRs and hypomethylated regions (with 250-bp flanking the start and end). The list of motif IDs (and corresponding names) that were included in the analysis are shown below:

MA0018.1	CREB1
MA0018.3	CREB1
MA0028.2	ELK1
MA0058.1	MAX
MA0058.3	MAX
MA0059.1	MAX::MYC
MA0062.1	GABPA
MA0093.2	USF1
MA0095.1	YY1
MA0095.2	YY1
MA0099.3	FOS::JUN
MA0104.4	MYCN
MA0136.2	ELF5
MA0149.1	EWSR1-FLI1
MA0156.2	FEV
MA0464.2	BHLHE40
MA0470.1	E2F4
MA0473.1	ELF1
MA0473.2	ELF1
MA0474.2	ERG
MA0475.1	FLI1
MA0475.2	FLI1
MA0476.1	FOS
MA0477.1	FOSL1
MA0478.1	FOSL2

MA0495.2	MAFF
MA0511.2	RUNX2
MA0526.1	USF2
MA0526.2	USF2
MA0636.1	BHLHE41
MA0638.1	CREB3
MA0640.1	ELF3
MA0641.1	ELF4
MA0649.1	HEY2
MA0663.1	MLX
MA0664.1	MLXIPL
MA0736.1	GLIS2
MA0749.1	ZBED1
MA0750.1	ZBTB7A
MA0750.2	ZBTB7A
MA0757.1	ONECUT3
MA0759.1	ELK3
MA0761.1	ETV1
MA0762.1	ETV2
MA0763.1	ETV3
MA0764.1	ETV4
MA0765.1	ETV5
MA0772.1	IRF7
MA0821.1	HES5
MA0822.1	HES7

MA0823.1	HEY1
MA0830.1	TCF4
MA0831.1	TFE3
MA0831.2	TFE3
MA0834.1	ATF7
MA0835.1	BATF3
MA0839.1	CREB3L1
MA0871.1	TFEC
MA1126.1	FOS::JUN(var.2)
MA1127.1	FOSB::JUN
MA1128.1	FOSL1::JUN
MA1129.1	FOSL1::JUN(var.2)
MA1130.1	FOSL2::JUN
MA1131.1	FOSL2::JUN(var.2)
MA1134.1	FOS::JUNB
MA1135.1	FOSB::JUNB
MA1136.1	FOSB::JUNB(var.2)
MA1137.1	FOSL1::JUNB
MA1138.1	FOSL2::JUNB
MA1139.1	FOSL2::JUNB(var.2)
MA1141.1	FOS::JUND
MA1142.1	FOSL1::JUND
MA1143.1	FOSL1::JUND(var.2)
MA1144.1	FOSL2::JUND
MA1145.1	FOSL2::JUND(var.2)

Relationship between gene expression and chromatin accessibility. Peaks were first called on ATAC-seq using the MACS2 software suite (16) with the added parameters: -g hs -q 0.05 --broad --nomodel --extsize 200 --nolambda. All peaks from each sample were then merged to provide one set of combined peaks. To count the number of reads overlapping peaks, we used featureCount (from the subread package) (17) with the following option: -p -P. For all downstream analyses, we excluded low-count peaks with an average read count lower than 10 across all samples, resulting in 79,282 peaks in total. We then plotted the distribution of changes in Tn5 accessibility (between non-infected and MTB-infected DCs across the five time-points of infection (2, 4, 18, 24, 48, and 72 hours)) for the top 25% most variable peaks associated with DE genes in each cluster. The DE genes associated with the selected peaks represent ~50% of the total genes within each of the DE clusters: (*i*) Early induced: 418/765 = 55%; (*ii*) Intermediate induced: 418/839 = 49%; and (*iii*) Persistent induced: 1083/2091 = 52%.

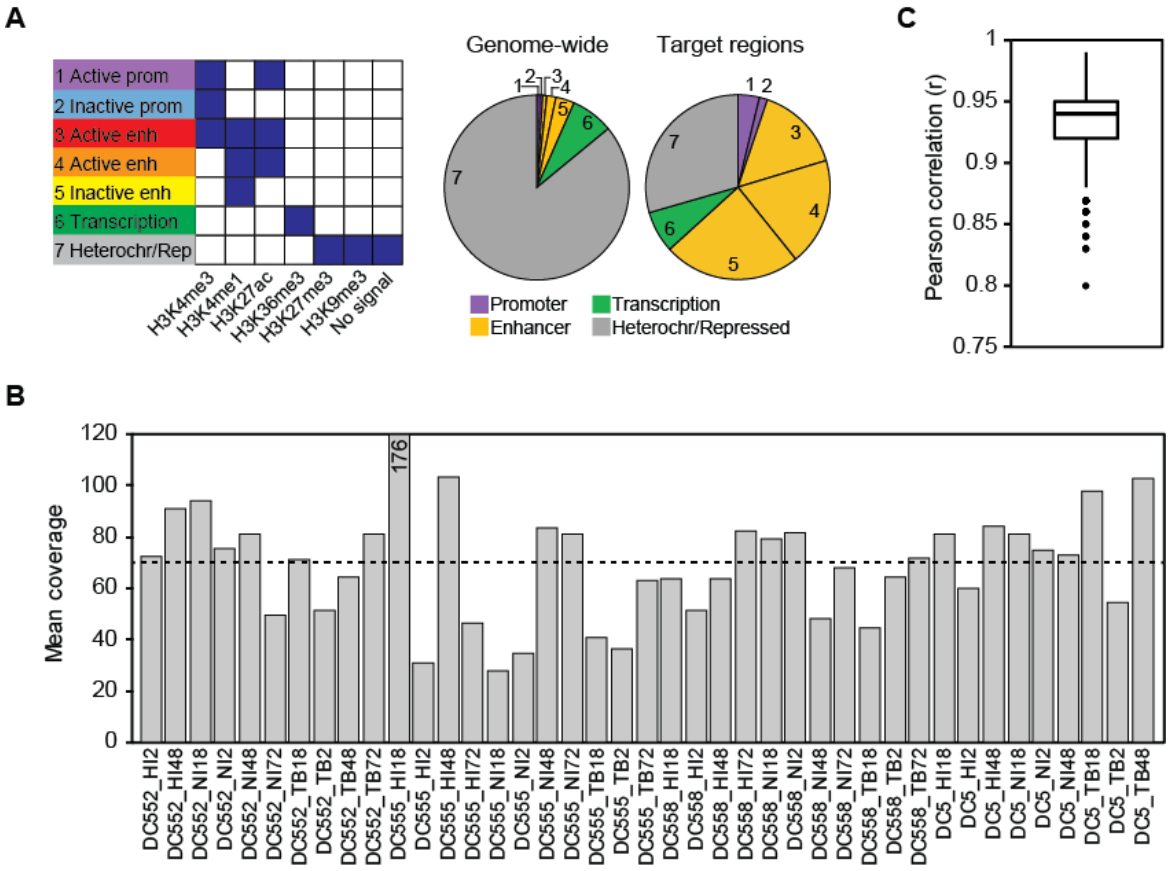

Fig. S1. Characteristics of SeqCap target regions. (*A*) Left: Combination of histone patterns used to define the 7 chromatin states (previously defined in (18)). Right: Pie charts showing the distribution of chromatin state annotations genome-wide and within SeqCap target regions in MTB-infected DCs. (*B*) Bar plots showing mean coverages of CpG sites within the target regions for each sample. Dotted line denotes the average coverage across all samples. (*C*) Correlation between DNA methylation levels at target regions among replicates (using only CpG sites with ≥5 coverage in all samples).

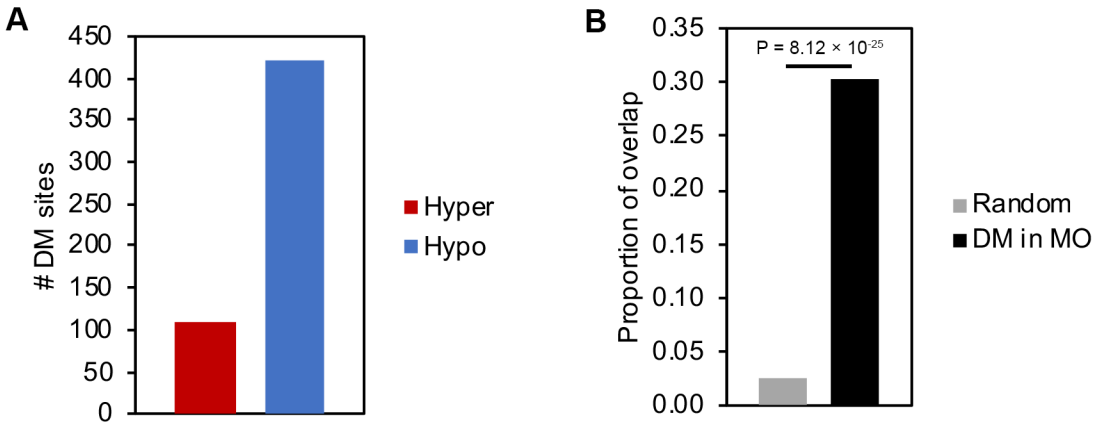

Fig. S2. (A) Barplots showing the absolute number of DM CpG sites identified in monocyte-derived macrophages at a |methylation difference| > 10% and FDR < 0.05 after MTB infection, either gains (red) or losses (blue). (B) Barplots comparing the overlap between DM CpG sites identified in monocyte-derived macrophages and DM CpG sites identified in DCs or random CpG sites in our SeqCapEpi panel.

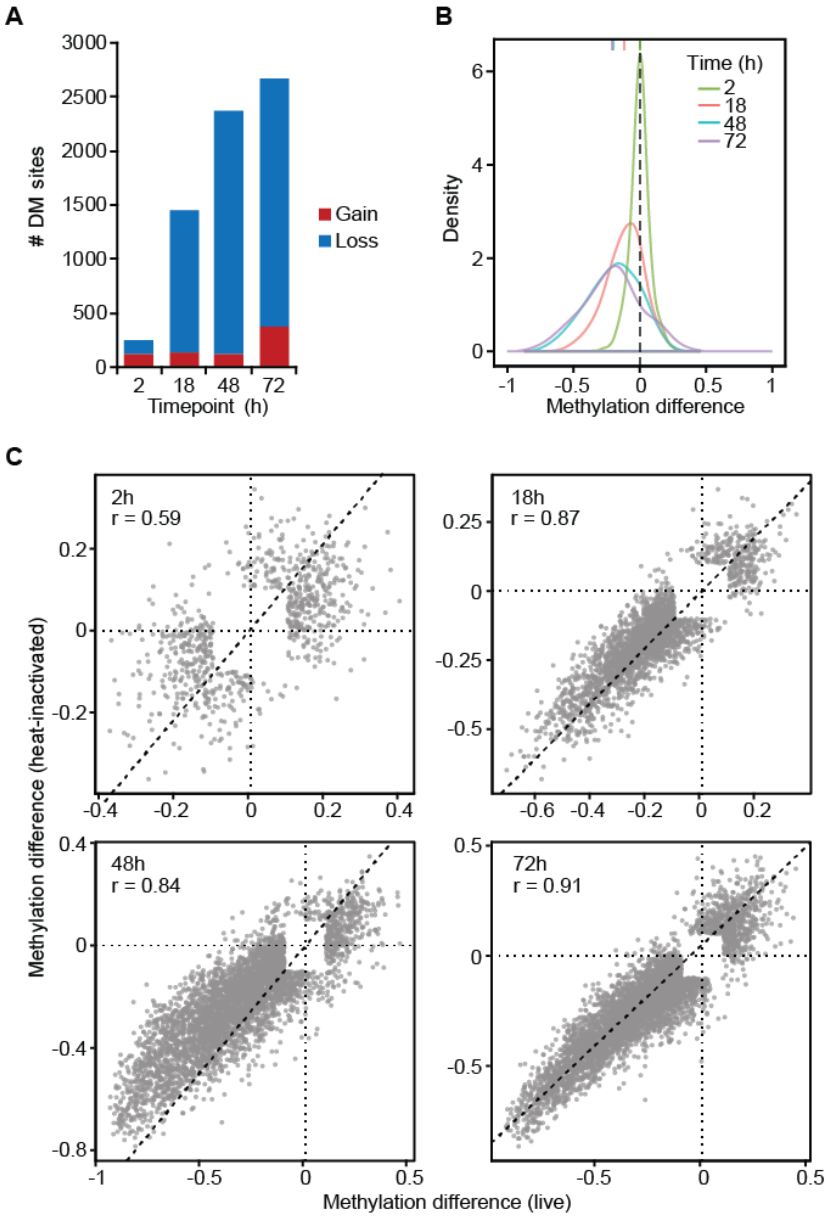

Fig. S3. DNA methylation dynamics in DCs in response to infection with heat-inactivated MTB. (*A*) Bar plots showing the number of differentially methylated sites identified at a |methylation difference| > 10% and FDR < 0.01 (y-axis) at each time point after infection with heat-inactivated MTB (2, 18, 48 and 72 hours (h); x-axis). (*B*) Distribution of differences in methylation between infected and non-infected cells at DM sites, at each time point. (*C*) Scatterplots depicting the correlation between differences in methylation in response to live (x-axis) or heat-inactivated MTB (y-axis) at each time point after infection (2, 18, 48 and 72 hours (h)).

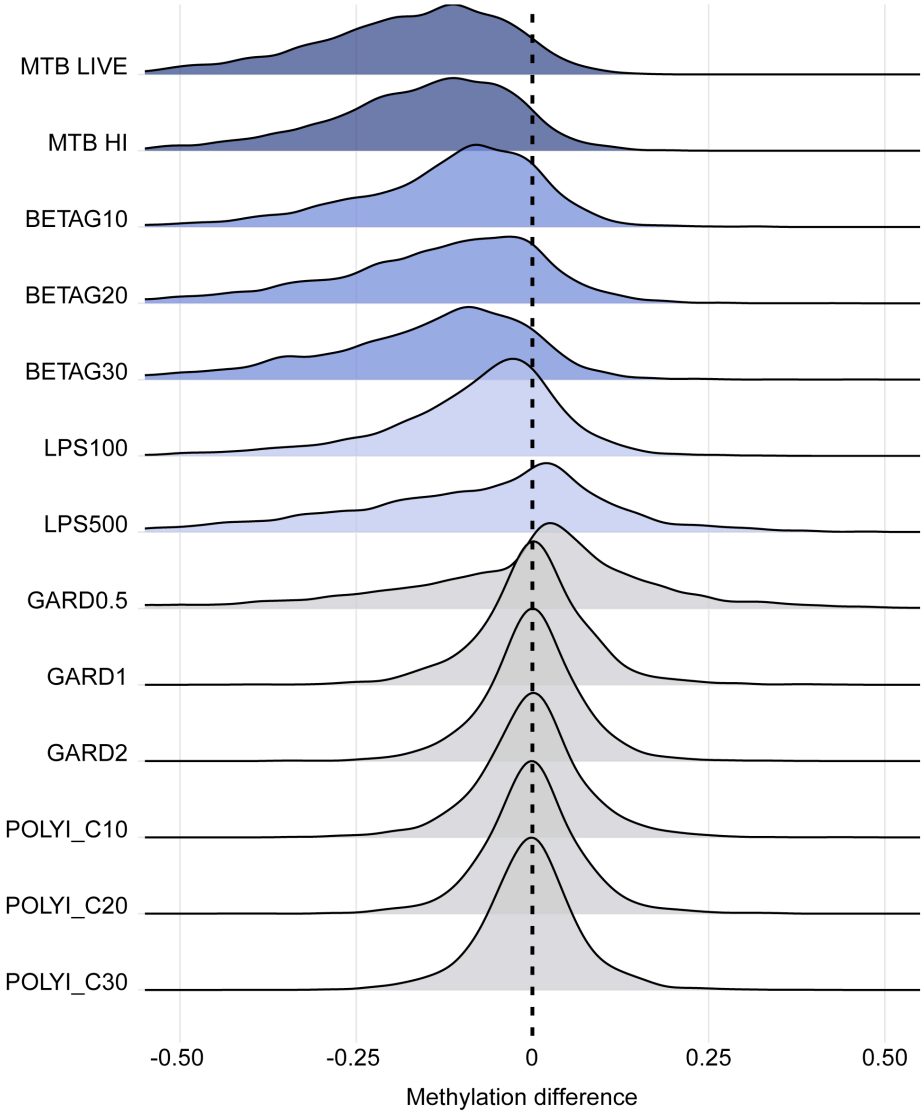

Fig. S4. Distribution of methylation changes in DCs stimulated various ligands for 24 hours – beta-glucan 10, 20, 30 ug/mL, LPS 100, 500 ng/mL, gardiquimod 0.5, 1, 2 ug/mL, poly I:C 10, 20, 30 ug/mL – among the 3,779 DM CpG sites identified in DCs after infection with live or heat-killed TB.

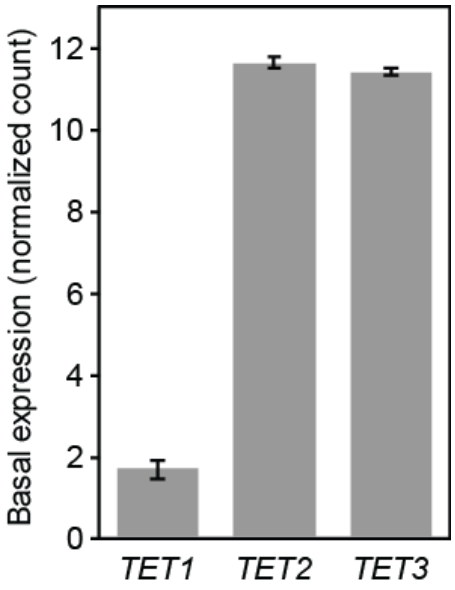

Fig. S5. Expression of *TET* genes in non-infected DCs. Bar plots showing the expression levels (in log2-normalized read counts) of *TET* genes, in non-infected DCs. All data are represented as mean ± s.e.m.

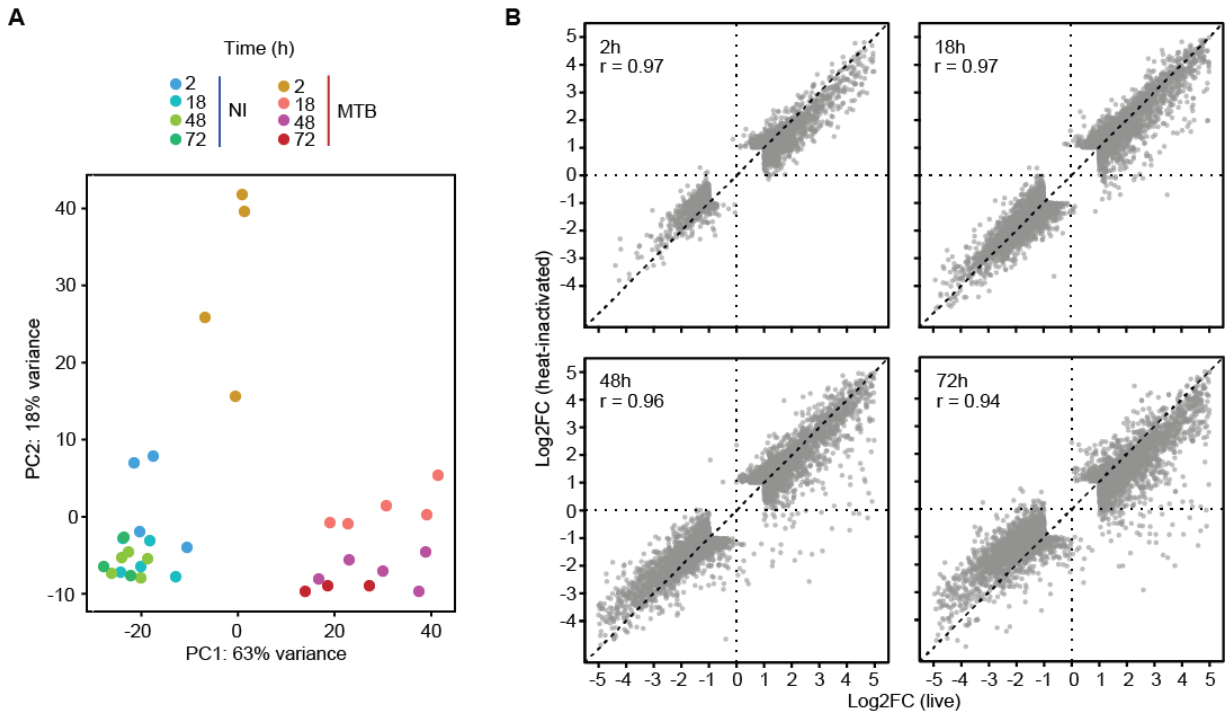

Fig. S6. Time course analysis of gene expression in DCs in response to infection with heat-inactivated MTB. (*A*) Principal component analysis of gene expression data from all samples. PC1 (x-axis) and PC2 (y-axis) clearly separate non-infected DCs from DCs infected with live MTB. (*B*) Scatterplots depicting the correlation between changes in expression (log2 fold changes) in response to live (x-axis) or heat-inactivated MTB (y-axis) at each time point after MTB infection (2, 18, 48 and 72 hours (h)).

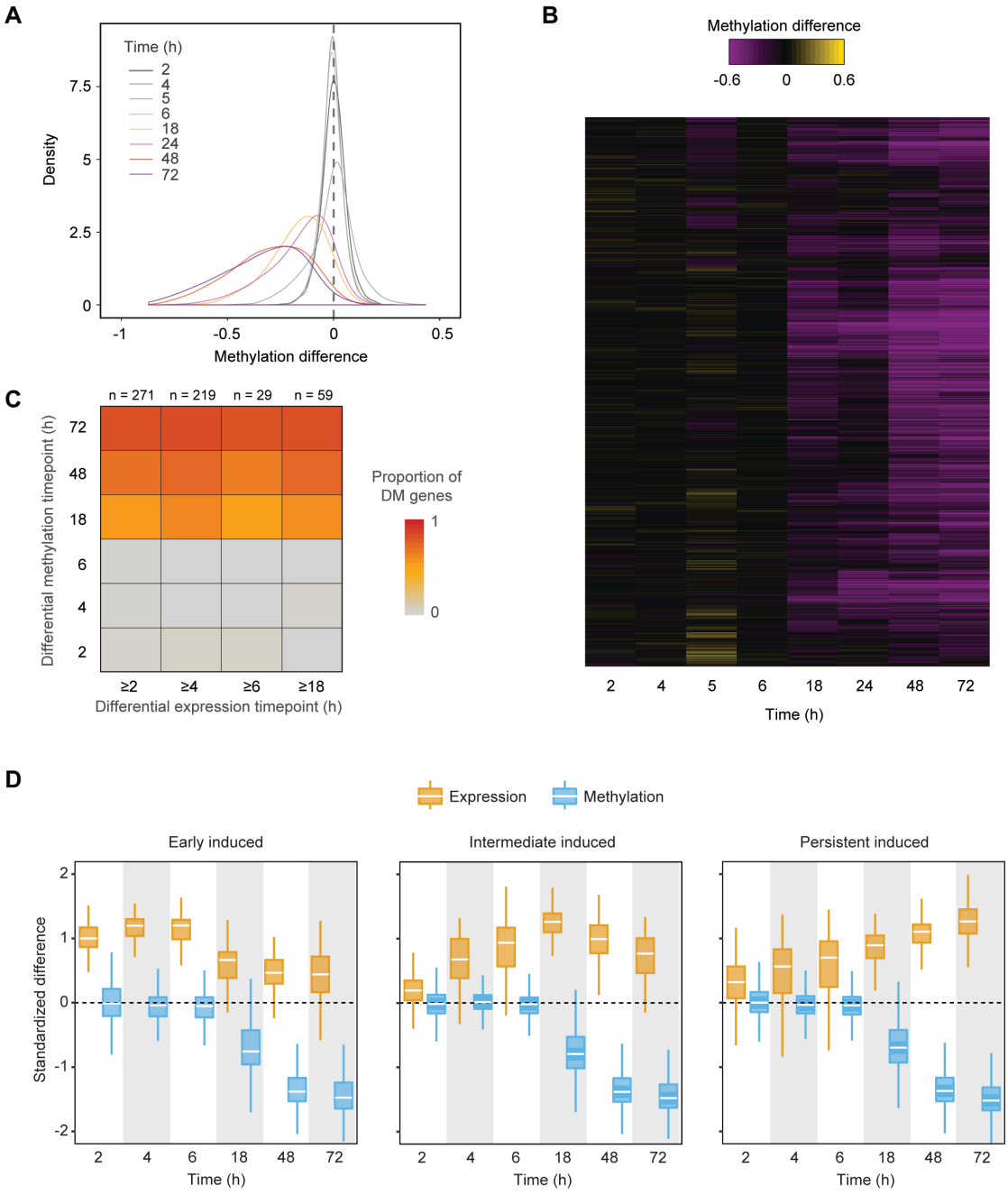

Fig. S7. (A) Distribution of differences in methylation between infected and non-infected cells at DM sites, at each time point. (B) Heatmap of differences in methylation DM sites (those defined in Cluster 3 in **Figure 1C**) across eight time points after infection. (C) Heatmap showing the proportion of genes associated with methylation changes at different time point (y-axis) among genes that start changing gene expression levels at 2-, 4-, 6, or 18-hours. The figure only contains genes that are associated with both changes in methylation and gene expression at any time point (5-hours is not included because we did not collect expression data for that time point). For example, 271 genes are already significantly up-regulated at 2 hours (FDR<1%); yet, only after 18 hour we start seeing a significant proportion of these genes also being associated with detectable changes in methylation. (D) Boxplots showing the distribution of standardized differences in methylation of DM sites in Cluster 3 (blue) along with the corresponding standardized differences in expression of the associated genes (orange), across all time points (x-axis).

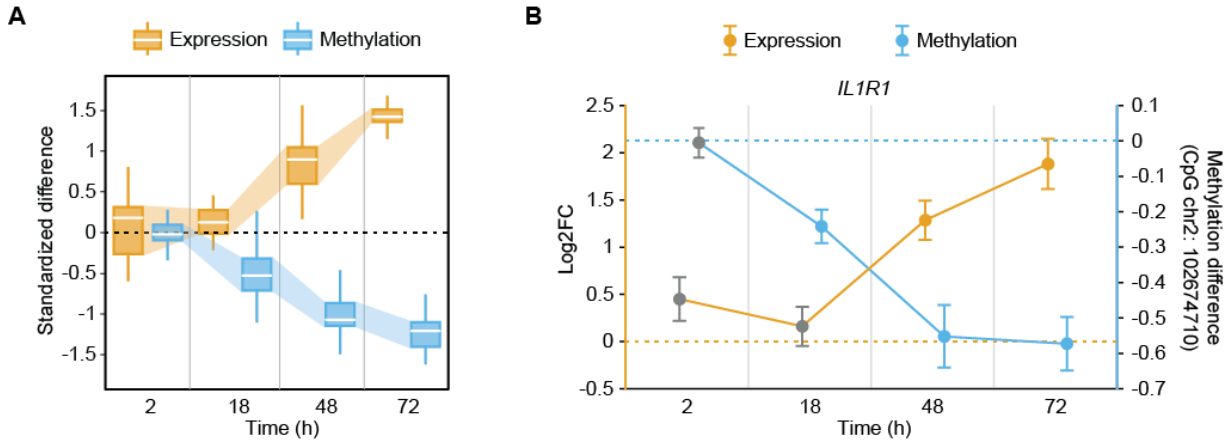

Fig. S8. Example of genes for which DNA demethylation occurred prior to gene activation. (*A*) Boxplots showing the distribution of standardized differences in methylation (blue) of Cluster 3 DM sites along with the corresponding standardized differences in expression (orange) of the associated genes, for which DNA demethylation occurred prior to gene activation (i.e., not differentially expressed after 2 and 18 hours post-infection using a relaxed FDR ≥ 0.1; n = 8 genes). These distributions are shown for each time point after MTB infection (2, 18, 48 and 72 hours (h)). (*B*) Specific example of changes in DNA methylation levels (blue; right y-axis) across all time points, along with the corresponding fold changes in log2 scale (orange; left y-axis) in expression of the associated gene that is induced after loss of methylation (defined in (*A*)). All data are represented as mean ± s.e.m. Gray dots denote no significant change in gene expression or methylation.

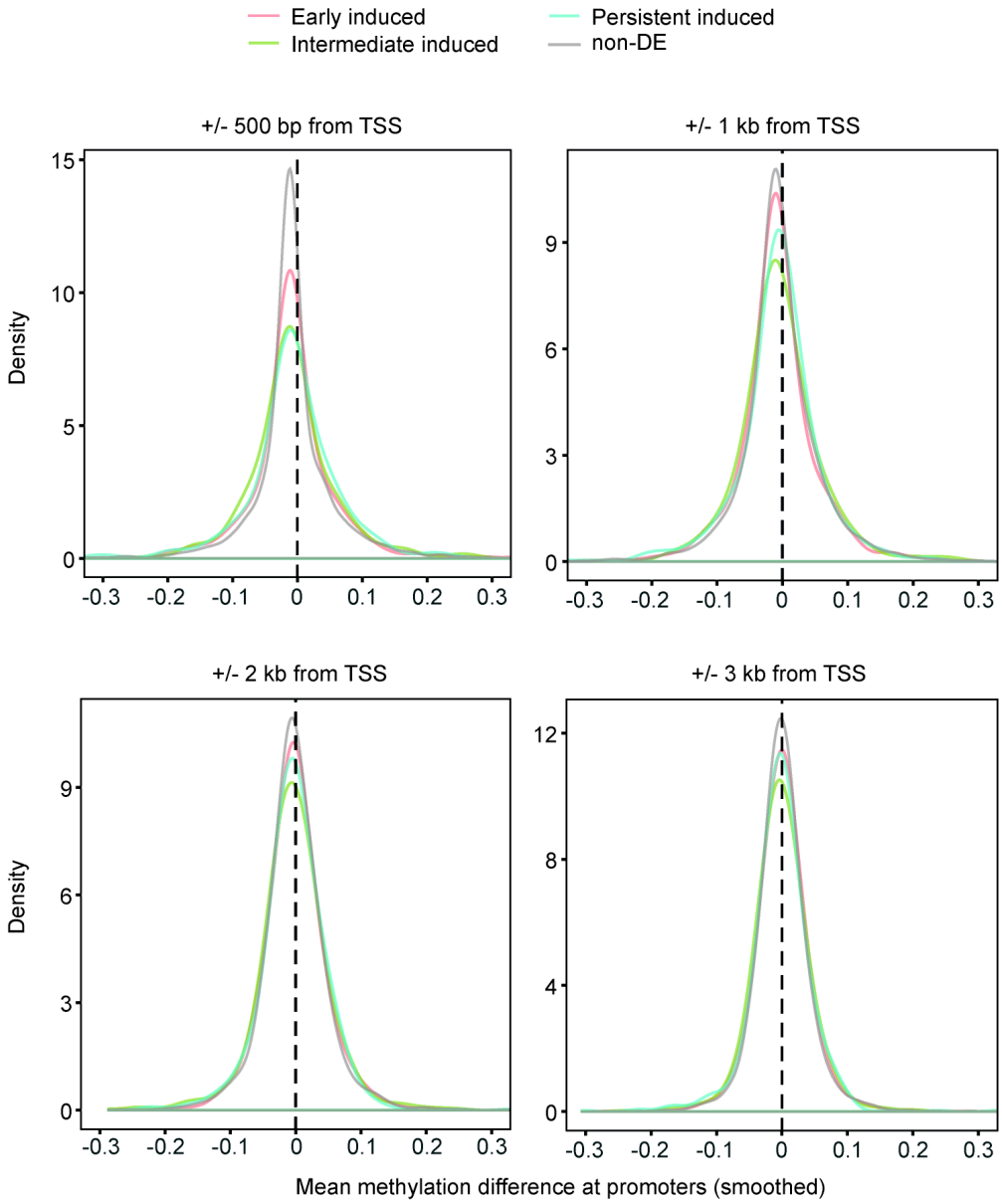

Fig. S9. Density plot of the average methylation differences (x-axis) observed in promoter regions (defined using different window sizes around the transcription start site (TSS)) between non-infected DCs and DCs infected with MTB for 2 hours. No noticeable differences in methylation changes were observed between the promoter of non-DE genes, and genes that are up-regulated upon MTB infection, regardless of their response dynamics.

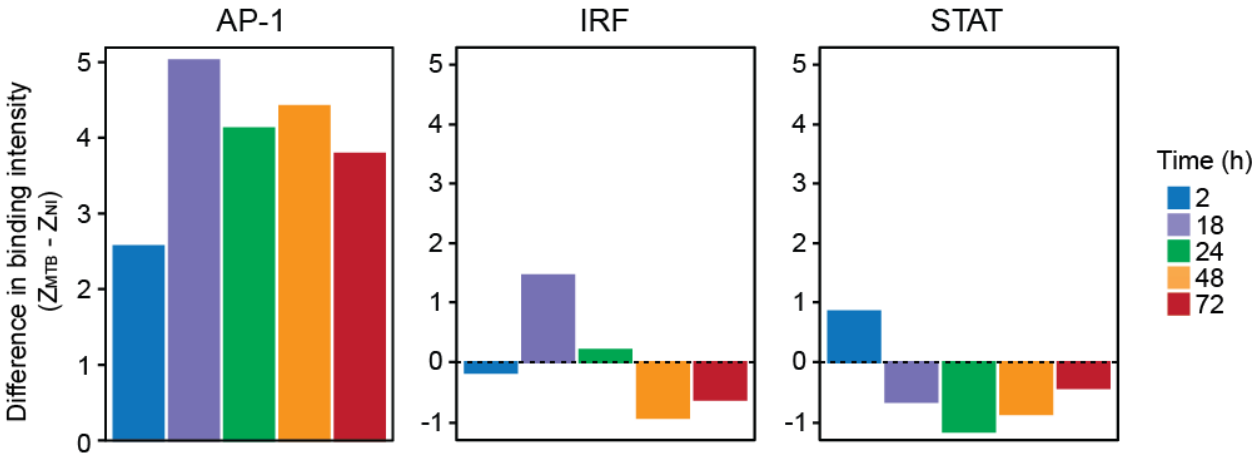

Fig. S10. Binding profiles of immune-related transcription factors within hypomethylated regions. Bar plots showing differences in TF occupancy score predictions for AP-1, IRF or STAT motifs between MTB-infected and non-infected DCs (Z_{MTB} - Z_{NI}; y-axis; see Methods), across four time points after infection (in hours (h); x-axis; see Methods). A positive Z-score difference indicates increased TF binding in hypomethylated regions after MTB infection.

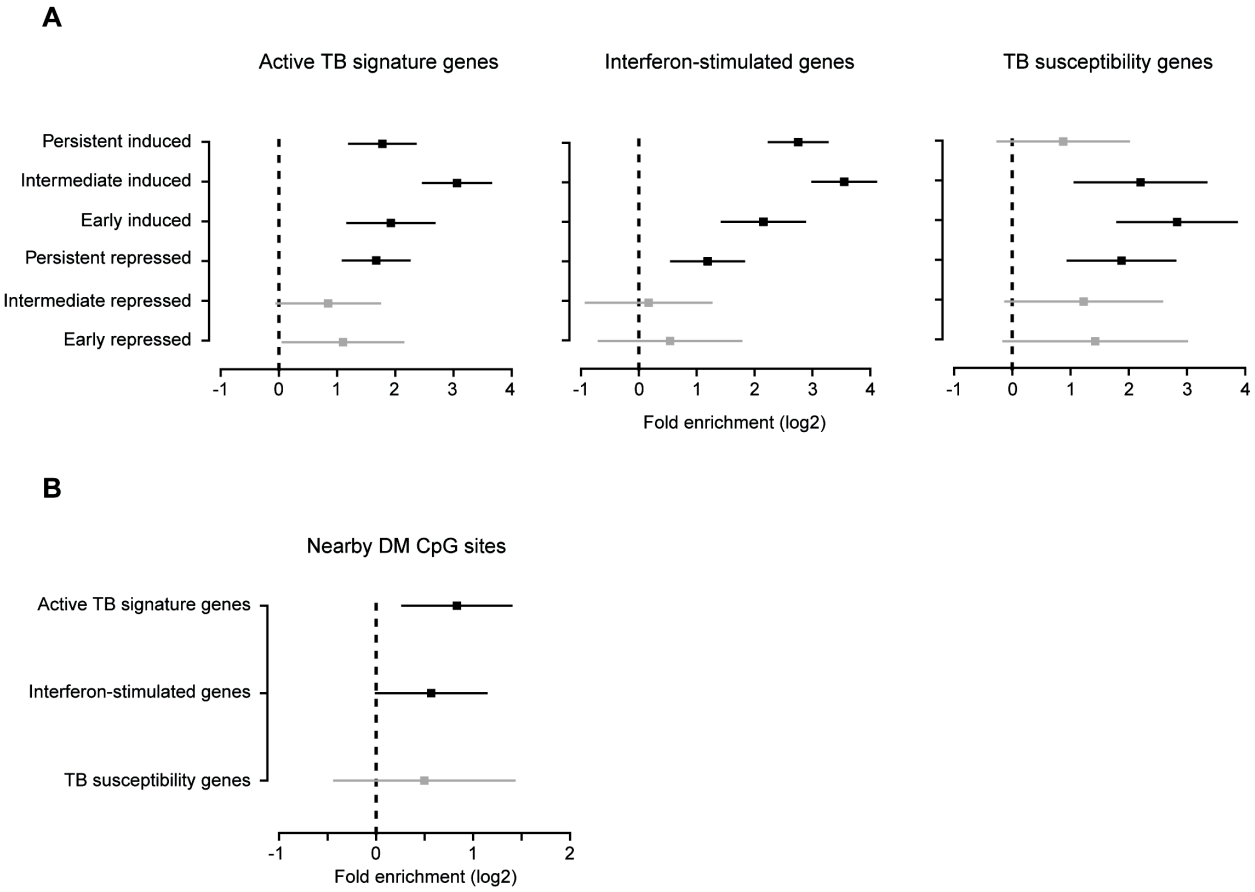

Fig. S11. (A) Enrichment (in log2; x-axis) of differentially expressed genes associated with active TB signature genes, interferon-stimulated genes in DCs, or TB susceptibility genes. Error bars show 95% confidence intervals for the enrichment estimates. (B) Enrichment (in log2; x-axis) of active TB signature genes, interferon-stimulated genes in DCs and TB susceptibility genes nearby (±100 kb) DM CpG sites (cluster 3). Black lines show enrichments at $P < 0.01$ and gray lines $P \geq 0.01$.

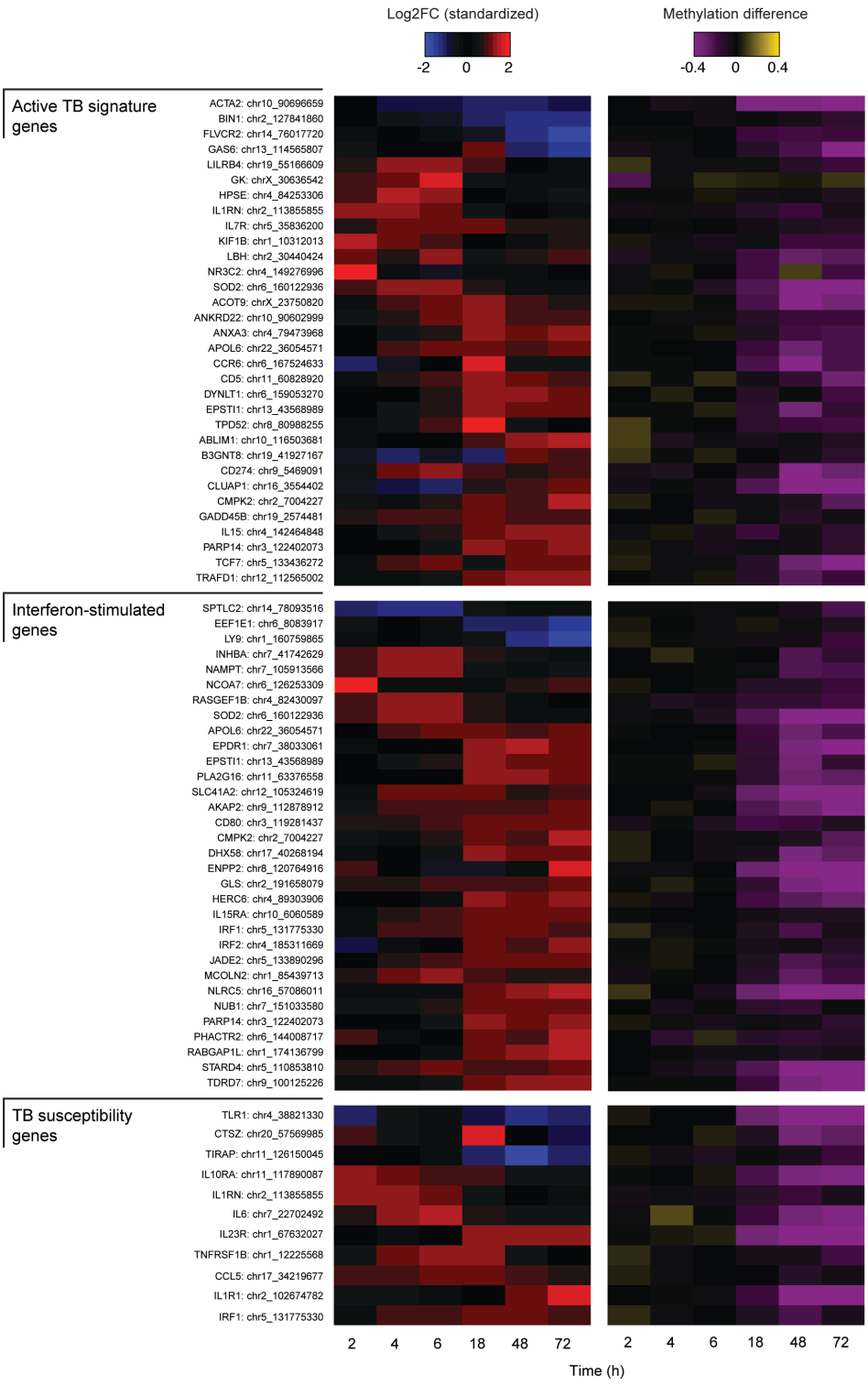

Fig. S12. Heatmaps showing differences in gene expression (left) and methylation (right) over time. The heatmaps only include genes for which we observe both a change in gene expression and a change in methylation status of one or more CpG sites. If more than one CpG sites was associated with a change in methylation, methylation changes are shown for the CpG site showing the most significant change in methylation.

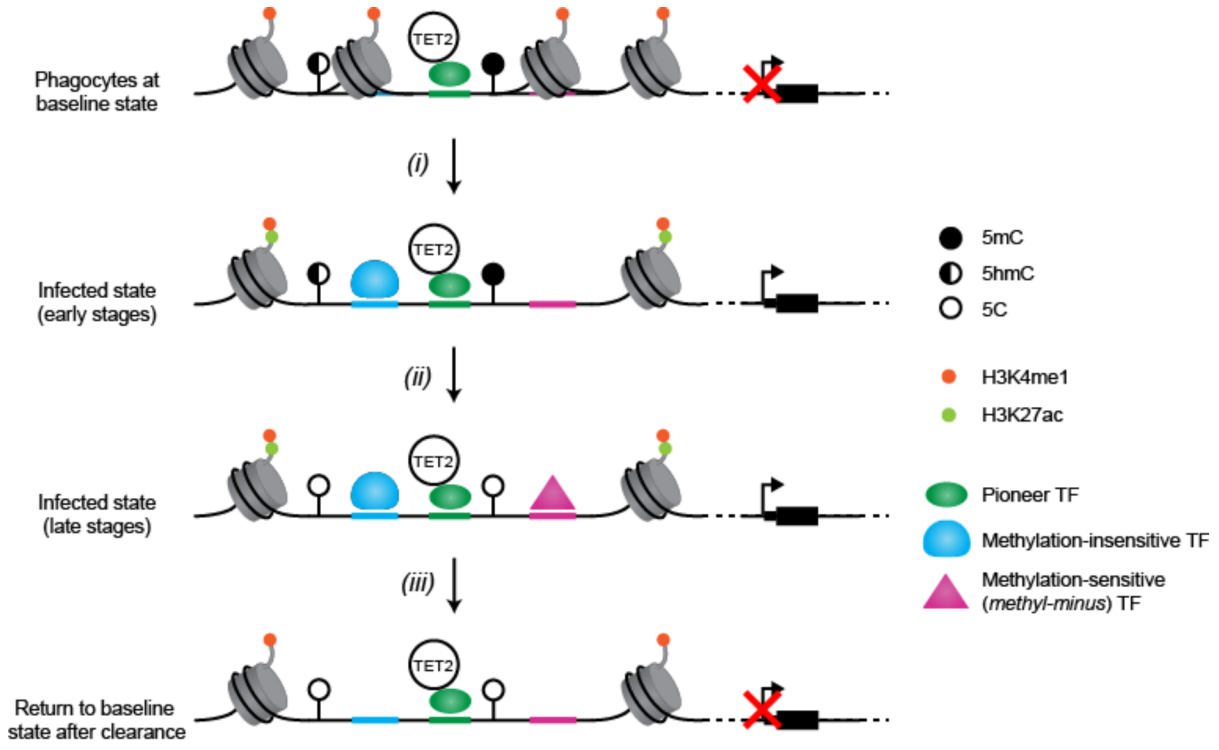

Fig. S13. Proposed model for the role of DNA methylation in innate immune responses to infection. Infection of phagocytes, such as DCs and macrophages, triggers the recruitment of signal-dependent TFs (specifically methylation-insensitive TFs) within the cell type-specific enhancer repertoires pre-established (marked by H3K4me1) by pioneer TFs prior to immune stimulation. The rapid binding of methylation-insensitive TFs during early stages of infection induces local chromatin opening, the recruitment of histone acetyltransferase p300, and the subsequent deposition of activating H3K27ac marks in these regions(19). The finding that DM CpG sites are highly enriched for 5hmC at baseline suggests that these sites are pre-bound by Ten-eleven Translocation (TET) enzymes, possibly via the pioneer factor PU.1(20). In this scenario, p300 then acetylates TET2, the most highly expressed TET enzyme in DCs and macrophages, which confers enhanced enzyme activity(21) and might account for the rapid loss of DNA methylation in response to infection. Removal of methylation marks allows the binding of methylation-sensitive (methyl-minus) TFs, which in turn induces expression of genes that play a role in later stages of infection. Importantly, loss of methylation at DM CpG sites persists even after immune stimulation has ceased. This phenomenon may contribute to the faster and stronger transcriptional response observed upon restimulation (i.e., trained immunity). 5mC: 5-methylcytosine, 5hmC: 5-hydroxymethylcytosine, 5C: (unmethylated) cytosine.

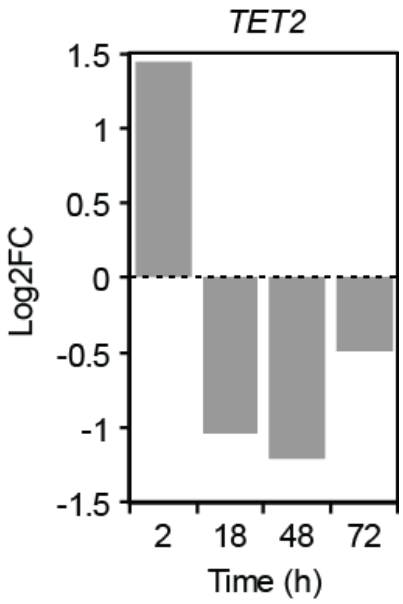

Fig. S14. *Tet2* expression profile in MTB-infected DCs. Bar plots showing changes in expression levels (in log2) of *Tet2*, across four time points after MTB infection (in hours (h); x-axis).

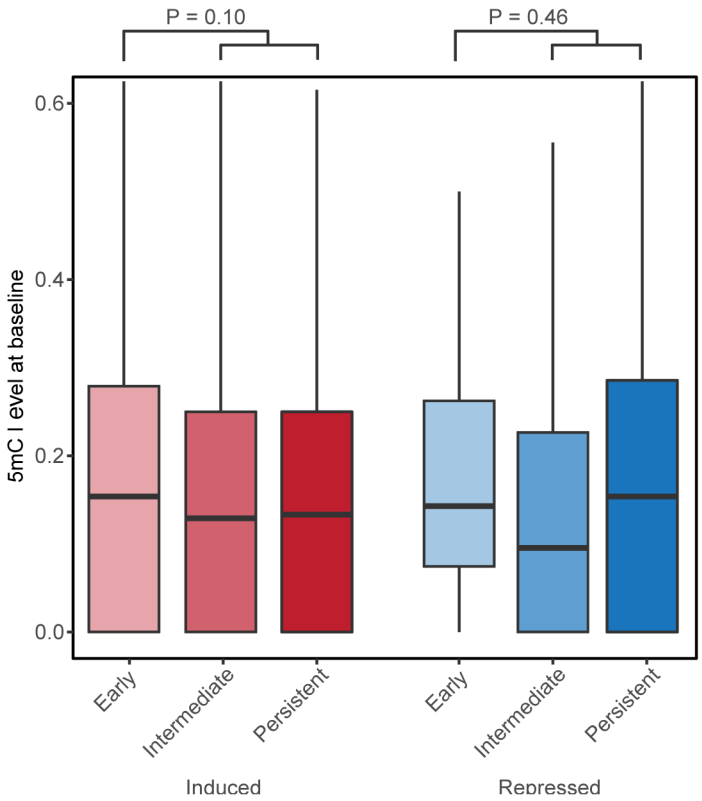

Fig. S15. (A) Boxplots comparing the distribution of 5hmC levels (y-axis) in non-infected DCs in DM sites associated with the different clusters of DE genes (x-axis). (B) Density plot of 5hmC levels (x-axis) in non-infected DCs in DM sites associated with the different clusters of induced DE genes.

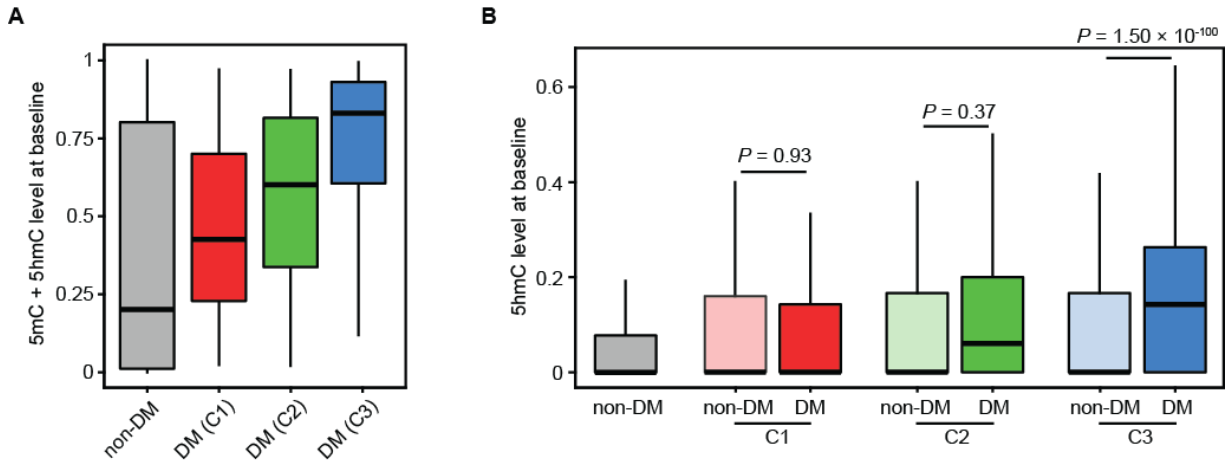

Fig. S16. 5hmC enrichment in differentially methylated (DM) CpG sites. (*A*) Boxplots of methylation levels (5mC + 5hmC) of non-DM and DM sites (Clusters 1, 2 and 3), in non-infected DCs. (*B*) Boxplots of 5hmC levels of all non-DM (gray) and DM sites in each cluster. Also shown are distributions of 5hmC levels using a random set of non-DM sites that matches the distribution of methylation found in non-infected samples within each set of DM sites (shown in (*A*)). Each random set contains the same number of CpG sites as those identified within each DM cluster.

SUPPLEMENTARY REFERENCES

1. Nedelec Y, *et al.* (2016) Genetic Ancestry and Natural Selection Drive Population Differences in Immune Responses to Pathogens. *Cell* 167(3):657-669 e621.
2. Buenrostro JD, Giresi PG, Zaba LC, Chang HY, & Greenleaf WJ (2013) Transposition of native chromatin for fast and sensitive epigenomic profiling of open chromatin, DNA-binding proteins and nucleosome position. *Nature methods* 10(12):1213-1218.
3. Pacis A, *et al.* (2015) Bacterial infection remodels the DNA methylation landscape of human dendritic cells. *Genome research*.
4. Krueger F & Andrews SR (2011) Bismark: a flexible aligner and methylation caller for Bisulfite-Seq applications. *Bioinformatics* 27(11):1571-1572.
5. Langmead B & Salzberg SL (2012) Fast gapped-read alignment with Bowtie 2. *Nature methods* 9(4):357-359.
6. Feng H, Conneely KN, & Wu H (2014) A Bayesian hierarchical model to detect differentially methylated loci from single nucleotide resolution sequencing data. *Nucleic acids research* 42(8):e69.
7. Hansen KD, Langmead B, & Irizarry RA (2012) BSmooth: from whole genome bisulfite sequencing reads to differentially methylated regions. *Genome biology* 13(10):R83.
8. Bray NL, Pimentel H, Melsted P, & Pachter L (2016) Near-optimal probabilistic RNA-seq quantification. *Nature biotechnology* 34(5):525-527.
9. Anders S, *et al.* (2013) Count-based differential expression analysis of RNA sequencing data using R and Bioconductor. *Nature protocols* 8(9):1765-1786.
10. Benjamini Y & Hochberg Y (1995) Controlling the False Discovery Rate: A Practical and Powerful Approach to Multiple Testing. *Journal of the Royal Statistical Society. Series B (Methodological)* 57(1):289-300.
11. Bindea G, *et al.* (2009) ClueGO: a Cytoscape plug-in to decipher functionally grouped gene ontology and pathway annotation networks. *Bioinformatics* 25(8):1091-1093.
12. Shen L, Shao N, Liu X, & Nestler E (2014) ngs.plot: Quick mining and visualization of next-generation sequencing data by integrating genomic databases. *BMC genomics* 15:284.
13. Li H & Durbin R (2009) Fast and accurate short read alignment with Burrows-Wheeler transform. *Bioinformatics* 25(14):1754-1760.
14. Khan A, *et al.* (2018) JASPAR 2018: update of the open-access database of transcription factor binding profiles and its web framework. *Nucleic acids research* 46(D1):D1284.
15. Yin Y, *et al.* (2017) Impact of cytosine methylation on DNA binding specificities of human transcription factors. *Science* 356(6337).
16. Zhang Y, *et al.* (2008) Model-based analysis of ChIP-Seq (MACS). *Genome biology* 9(9):R137.
17. Liao Y, Smyth GK, & Shi W (2014) featureCounts: an efficient general purpose program for assigning sequence reads to genomic features. *Bioinformatics* 30(7):923-930.
18. Pacis A, *et al.* (2015) Bacterial infection remodels the DNA methylation landscape of human dendritic cells. *Genome research* 25(12):1801-1811.
19. Bhatt D & Ghosh S (2014) Regulation of the NF-kappaB-Mediated Transcription of Inflammatory Genes. *Front Immunol* 5:71.
20. de la Rica L, *et al.* (2013) PU.1 target genes undergo Tet2-coupled demethylation and DNMT3b-mediated methylation in monocyte-to-osteoclast differentiation. *Genome Biol* 14(9):R99.
21. Zhang YW, *et al.* (2017) Acetylation Enhances TET2 Function in Protecting against Abnormal DNA Methylation during Oxidative Stress. *Mol Cell* 65(2):323-335.